INTERNATIONAL JOURNAL OF NUMERICAL MODELLING: ELECTRONIC NETWORKS, DEVICES AND FIELDS
Int. J. Numer. Model. 2010; **23**:301–314
Published online 6 November 2009 in Wiley InterScience (www.interscience.wiley.com). DOI: 10.1002/jnm.731

Enhanced Terahertz detection in self-switching diodes

I. Iñiguez-de-la-Torre[1,*,†], J. Mateos[1], D. Pardo[1], A. M. Song[2] and T. González[1]

[1]*Departamento de Física Aplicada, Universidad de Salamanca, Plaza de la Merced s/n, 37008 Salamanca, Spain*
[2]*School of Electrical and Electronic Engineering, University of Manchester, Manchester M60 1QD, U.K.*

SUMMARY

In this work, by means of Monte Carlo simulations, we analyze the presence of a resonance in the DC current response of an asymmetric nonlinear nanodiode (called self-switching diode) to AC voltage excitations in the Terahertz range. The phenomenon, which takes place at room temperature, can be enhanced and tuned by the geometry of the device, being potentially useful for selective Terahertz detection. The resonance is linked to a noise mechanism: collective charge fluctuations in the space-charge region around the active channel of the device, which are visible both in noise and rectification. The enhancement of the DC current is attributed to the phase shift between the applied signal and the response of the charge around the channel near the vertical trenches, which controls the electron flow through the diode. Copyright © 2009 John Wiley & Sons, Ltd.

Received 11 November 2009; Revised 28 July 2009; Accepted 7 September 2009

KEY WORDS: Monte Carlo simulation of nanodevices; Terahertz detectors

1. OVERVIEW OF THE DEVICE

In recent years the Terahertz range of the electromagnetic spectrum has gained international interest due to its broad potential applications, ranging from ultra-high-speed optical transmission systems to medical diagnostic, industrial quality control or security-screening tools [1]. Therefore, the development of compact and low-cost semiconductor devices covering the THz band is one of the challenges of nanoelectronics in a medium term future. Great efforts are being made to build compact THz devices operating at room temperature, based on different physical effects. Among them, collective phenomena seem to be a promising possibility. For

*Correspondence to: I. Iñiguez-de-la-Torre, Departamento de Física Aplicada, Universidad de Salamanca, Plaza de la Merced s/n, 37008 Salamanca, Spain.
†E-mail: indy@usal.es

Contract/grant sponsor: Dirección General de Investigación (MEC, Spain); contract/grant number: TEC2007-61259/MIC
Contract/grant sponsor: Consejería de Educación of the Junta de Castilla y León (Spain); contract/grant number: SA019A08

example, plasma oscillations in the two-dimensional electron gas of nanometer field effect transistors have been explored in the last years in order to develop THz emitters and detectors [2–4]. Transit time resonance assisted by optical phonon emission in wide bandgap semiconductors and related plasma instabilities are another alternative, predicted by theory and confirmed by simulations [5, 6]. A recently developed planar asymmetric nonlinear nanodevice, called self-switching diode (SSD), is also a promising candidate to operate in the THz range [7], as we will illustrate in this work. The SSD is fabricated with just one lithographic step, by simply etching L-shaped insulating grooves onto a semiconductor layer, thus defining a narrow channel with broken symmetry, as shown in Figure 1. This topology provides an attractive rectifying I–V characteristic (without the use of any doping junction or barrier structure) with a threshold voltage that can be tuned from almost zero to more than 10 V by adjusting the channel width and other geometric parameters. This behavior has been explained by Monte Carlo (MC) simulations [8].

A key aspect of these nanodevices is their planar geometry, which provides important advantages when operating at high frequency: reduced parasitic capacitances between contacts with respect to conventional vertical devices of the same size, feasibility to integrate many SSDs in parallel without the need of interconnects (thus overcoming the high-impedance problems typical of nanodevices, which limit their extrinsic frequency performance), flexible design that allows for an optimized heat management and frequency tuning when operating as THz sources, and very simple integration with antennas to improve emitted power and detection sensitivity. Additionally, the downscaling of these devices is very simple, which, combined with the use of high mobility semiconductors for the channel, such as InGaAs, InAs or InSb (allowing for ballistic transport), may envisage the fabrication of devices working in the THz range as power detectors or frequency multipliers. Experiments in InGaAs diodes have demonstrated microwave detection up to 110 GHz at 300 K [9] and up to 2.5 THz at low temperature [10].

MC models have been proved to be quite useful for the analysis of the static, dynamic and noise behavior of SSDs [8, 11–13]. In this work we will analyze the high-frequency behavior of SSDs operating as detectors by means of MC simulations. We will mainly focus our attention on a high-frequency collective phenomenon that leads to a tunable-by-geometry peak in the SSDs current noise spectrum and couples to the DC response of the device, thus originating a THz resonance in the rectification of AC signals that could be very useful for applications.

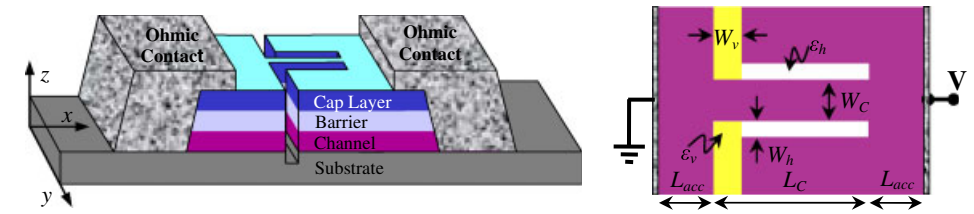

Figure 1. (a) 3D schematic view of a SSD including the details of the heterostructure used in the fabrication and (b) top-view geometry (xy plane) considered in the 2D MC simulations. W_C channel width, L_C channel length, W_v and W_h width of the vertical and horizontal trenches, ε_v and ε_h permittivity of the vertical and horizontal trenches and L_{acc} length of the accesses to the channel.

DOI: 10.1002/jnm

2. MONTE CARLO MODEL

A semi classical MC method self-consistently coupled with a Poisson solver is used in our analysis [14]. Three nonparabolic spherical valleys are considered: Γ, L and X. Accurate scattering models for ionized impurities, polar and nonpolar optical phonons, acoustic phonons and intervalley processes are taken into account. The analysis of SSDs would require a 3D simulation with the topology shown in Figure 1(a) to exactly describe the influence of the lateral surface charges and the actual layer structure. To avoid the complexity of 3D models, here instead we perform 2D simulations only in the InGaAs channel (Figure 1(b)), and the influence of the fixed charges present in other layers is accounted for by means of a 'background doping' [14]. As a result of the nanoscale dimensions of the device, the depletion of the channel originated by the action of the lateral surface charge at the semiconductor–air interfaces may have a dramatic influence in the final response of the device. Hence, we include this surface charge as a Neumann boundary condition for the Poisson equation. Since we are dealing with nanoscale devices where transport may be ballistic, contact injection is also a critical point, and the velocity distribution and time statistics of injected carriers must be accurately modelled [14].

The noise behavior and the dynamic response of the diodes can be straightforwardly studied by means of MC simulations, since the random microscopic processes source of fluctuations and the fluctuating electric potential are included in a natural way without any approximation. For the noise analysis we follow the standard scheme explained elsewhere [15]. From the instantaneous current values, obtained by using the generalized Ramo–Shockley theorem, the current autocorrelation function is calculated and, in virtue of the Wiener–Kintchine theorem, the corresponding spectral density is determined by Fourier transform.

Simulations are run at room temperature during 500 000 time steps of 1 fs each to calculate the noise, and during 200 000 steps of 1 fs to determine the DC response to AC excitations of different frequencies, ranging form 100 GHz to 5 THz.

3. RESULTS AND DISCUSSION

In this section we will show the influence of the geometry of the diode on its I–V characteristics and dynamic behavior. A pronounced resonant peak is observed in the frequency response of the devices, whose origin is explained by means of microscopic results jointly with the analysis of the noise spectra. Finally, we propose an equivalent circuit to confirm our interpretation.

3.1. Influence of the trenches' properties

The SSD under study consists of an $In_{0.53}Ga_{0.47}As$ channel with the 2D topology showed in the inset of Figure 1(b). We will investigate diodes with channel length $L_C = 250$ nm, channel width $W_C = 50$ nm, width of the horizontal trenches $W_h = 5$ nm, relative permittivity of the horizontal trenches $\varepsilon_h = 1$ and length of the accesses $L_{acc} = 175$ nm. Different values of the width of the vertical trenches W_v and of their relative permittivity ε_v will be investigated. As observed in the insets of Figure 2(a),(b), the nonlinearity exhibited by the I–V curves is insensitive to the properties of the vertical trench, i.e. the values of W_v and ε_v. The reason is that the self-switching effect is based on the transverse coupling of electric field to the nanochannel across the horizontal trenches [8].

DOI: 10.1002/jnm

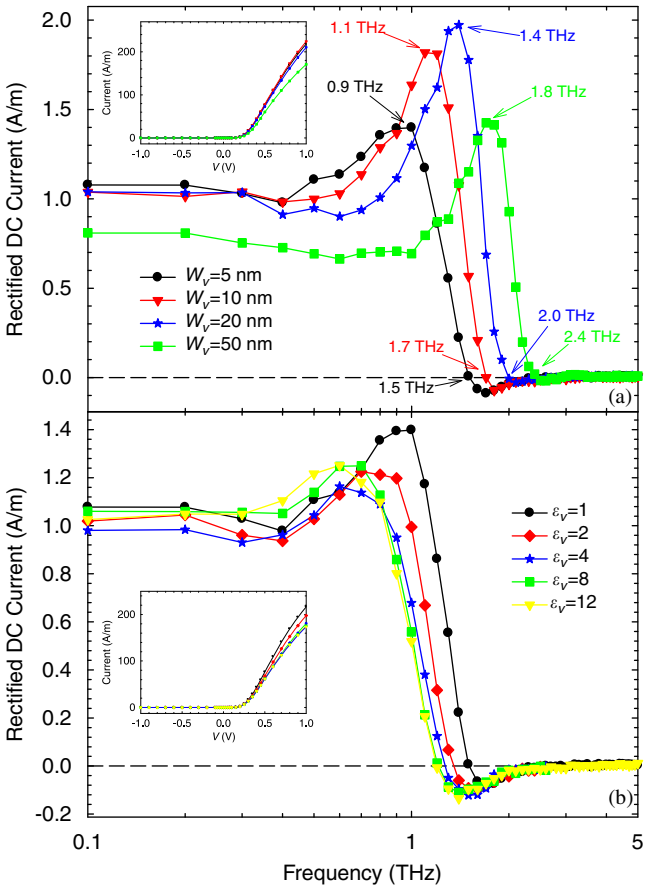

Figure 2. Mean current vs frequency of the applied AC voltage (amplitude of 0.25 V) in SSDs with the topology of Figure 1 for: (a) different values of W_v and $\varepsilon_v = 1$ and (b) different values of ε_v and $W_v = 5$ nm. $L_C = 250$ nm, $W_C = 50$ nm, $W_h = 5$ nm, $\varepsilon_h = 1$ and $L_{acc} = 175$ nm. Insets: I–V curves.

The dynamic behavior of devices can be tested by calculating the DC output current in response to sinusoidal input voltage signals, $V(t) = V_0\ \mathrm{sen}(2\pi ft)$, of increasing frequency f applied between the contacts. Figure 2(a) shows the results for SSDs with different widths of the vertical trenches W_v and $\varepsilon_v = 1$ (with $V_0 = 0.25$ V). As a general feature, a pronounced peak is observed after a flat region, just before the decay in the response. The frequency of the peak, f_p, is shifted to higher values for wider vertical trenches and the maximum rectified current can be as high as twice the value at low frequency. The peak is also sensitive to the permittivity of the vertical trenches ε_v, as observed in Figure 2(b), corresponding to SSDs where $W_v = 5$ nm and ε_v takes different values. In this case, f_p shifts to lower frequencies as ε_v is increased, saturating for $\varepsilon_v > 4$ (to be explained later). The observed dependence of f_p on W_v and ε_v suggests a strong influence of the capacitor associated with the vertical trenches $C_v = \varepsilon_v/W_v$ on the phenomenon originating the resonance; explaining the opposite effect of ε_v and W_v on f_p.

In order to confirm this explanation, different SSDs have been simulated varying the properties of the horizontal trenches. The position of the peak has been found to be insensitive

DOI: 10.1002/jnm

to W_h (Figure 3(a)) and ε_h (Figure 3(b)). Nevertheless, the turn-on voltage of the static I–V curve is influenced by the width of the horizontal trenches (see inset of Figure 3(a)), decreasing for smaller W_h. This is due to the stronger transverse electric field present for smaller W_h, which enables a more efficient control of the opening and closing of the nanochannel when biasing the anode. For this reason, in the dynamic analysis, to operate with approximately the same current level in the three diodes ($\sim$1.7 A/m), the excitation, in this case of $V_0 = 0.1$ V, is applied over a DC value of 0.185, 0.4 and 0.7 V for widths of 5, 10 and 20 nm, respectively. On the other hand, as observed in the inset of Figure 3(b), horizontal trenches filled with a high-k material would lead to an increase of the current (and a reduction of the threshold voltage). In this case an excitation applied over equilibrium but with $V_0 = 0.25$, 0.075 and 0.05 V, respectively, is used to provide similar values of current at low frequency.

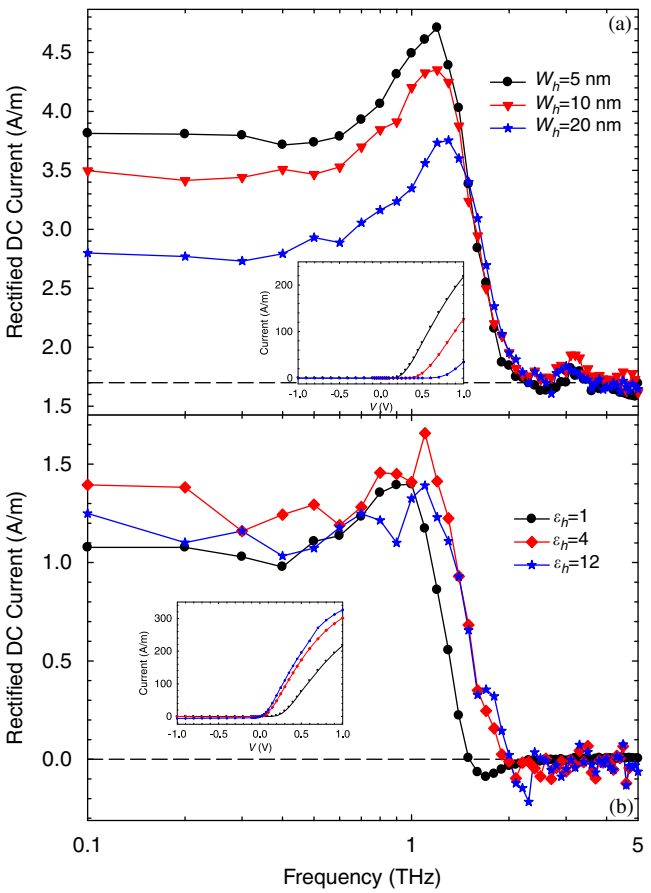

Figure 3. Mean current vs frequency of the applied AC voltage in SSDs with the topology of Figure 1 for: (a) different values of W_h and $\varepsilon_h = 1$ ($V_0 = 0.1$ V applied over a DC value of 0.185, 0.4 and 0.7 V, respectively) and (b) different values of ε_h and $W_h = 5$ nm ($V_0 = 0.25$, 0.075 and 0.05 V, respectively, applied over equilibrium). $L_C = 250$ nm, $W_C = 50$ nm, $W_v = 5$ nm, $\varepsilon_v = 1$ and $L_{acc} = 175$ nm. Insets: I–V curves.

DOI: 10.1002/jnm

3.2. Origin of the resonant peak

By means of the microscopic results of the MC simulation we can get to a better understanding of how the device works and identify the origin of the peak. Figure 4 shows the longitudinal profiles of electric potential along the center of the channel, exhibiting a barrier, induced by the charge at the surface states, which controls the electron flow between contacts. Owing to the asymmetry of the diode, the barrier is lowered much more by forward than by reverse applied biases, thus providing the rectifying behavior typical of SSDs, which is observed in the previous *I–V* curves. It can be observed that the minimum of the potential is located just at its left entrance, especially in diodes with wide vertical trenches when biased near the conduction threshold. This means that the regions of the diode that have the strongest influence on the modulation of the channel conductance, which could lead to the observed resonant peak in the DC rectified current, are those surrounding the channel close to the vertical trenches. Indeed, the amplitude of the potential barrier is strongly modulated by the charge variations within the outside surrounding regions (close to the vertical trenches), which are obviously regulated by C_v.

To explain this phenomenon, we propose a model, analogous to that of Reference [13], based on the time-dependent charging and discharging of those regions and their phase shift with respect to the electric potential dropped in the nanochannel. When the SSD is biased, the regions surrounding the channel will be charged or discharged, which results in the opening or closing of the nanochannel. To characterize these phenomena, we study the time-dependence of a parameter $\Delta(t,f)$ defined as:

$$\Delta(t,f) = \frac{N_{db} - n(t,f)}{N_{db} - n(0)} \tag{1}$$

with $n(t,f)$ and $n(0)$ being the carrier concentration at time t for an excitation frequency f and at equilibrium ($V = 0$ V), respectively, in the region within 50 nm at the right of the sidewall of the vertical trenches. N_{db} is the net doping assigned to the channel (with impurity scattering

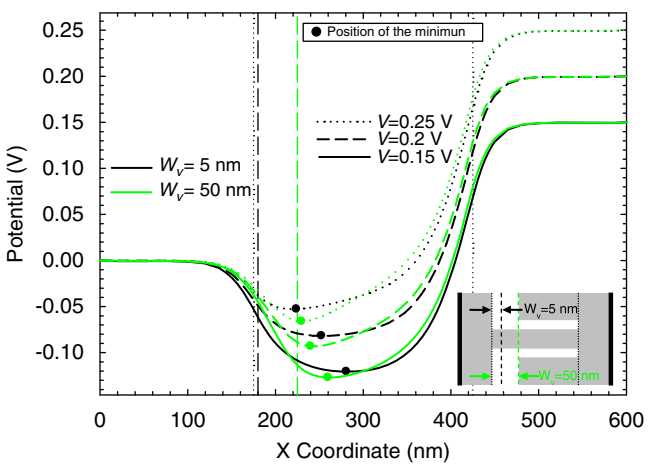

Figure 4. Profiles of electric potential along the center of the channel for different biases in diodes with $W_v = 5$ nm and $W_v = 50$ nm. The vertical dotted lines draw up the boundaries of the channel and the dashed ones indicate the width of the vertical trenches as sketched in the inset.

DOI: 10.1002/jnm

switched off) to correctly reproduce electron transport in our 2D simulator. With this definition, when $\Delta > 1$ the surroundings of the vertical trench are positively charged (channel opened) with respect to equilibrium conditions, and if $\Delta < 1$ there is an increase of negative charges in that region (channel closed). The frequency dependence of the phase shift $\delta\phi$ between Δ and the electric potential dropped in the nanochannel, together with the maximum exhibited by the amplitude of Δ (Figure 5(b)), provide the explanation for the peak in the rectification. Figure 5 shows the results for the same SSDs of Figure 2(a). If Δ and the potential drop are in phase, only in the positive half-period of the applied potential the diode will be opened, and vice versa, the diode will be closed when the bias is negative. These conditions correspond to the low-frequency flat region of the DC rectified current shown in Figure 2(a). A diphase leads to a reduction in the rectified current. However, a significant enhancement in the DC current after the *plateau* is observed. This is caused by the increase of Δ, which reaches its maximum value here. The peaks in Figure 2(a), indicated by arrows (0.9, 1.1, 1.4 and 1.8 THz), approximately coincide with $\delta\phi = \pi/4$ and the maximum of Δ in Figure 5(b). When $\delta\phi = \pi/2$, the channel will be opened only

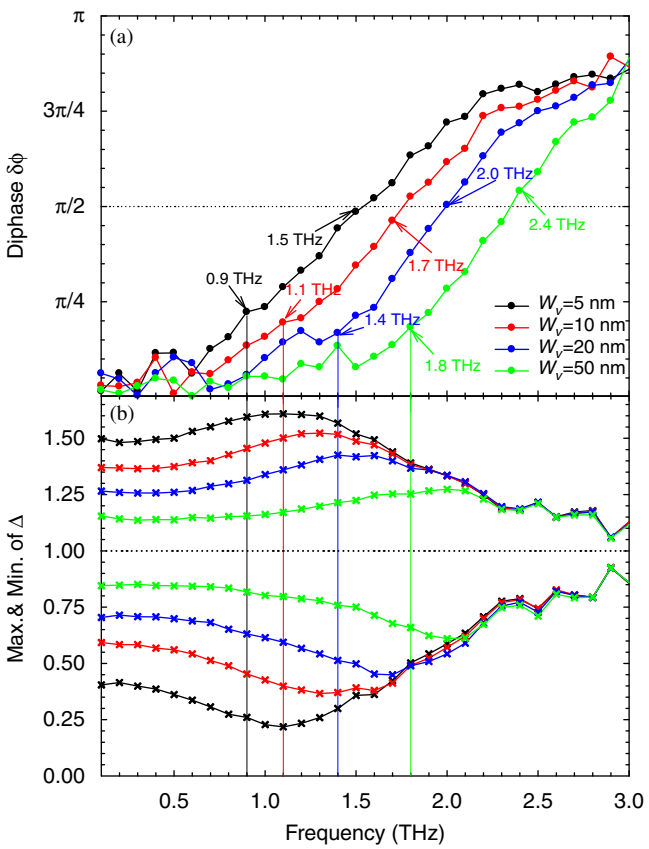

Figure 5. (a) Diphase $\delta\phi$ between Δ and the voltage dropped in the channel and (b) maximum and minimum of Δ as a function of the frequency of the AC signal applied to SSDs with $W_v = 5$, 10, 20 y 50 nm. The channel length is in all cases $L_C = 250$ nm. Vertical lines correspond to the position of the peak of the rectified DC current shown in Figure 2(a).

DOI: 10.1002/jnm

during the first and fourth quarter periods, while the potential dropped in the nanochannel (and the current flow) is half period negative and half period positive, so that the rectified current is zero. This situation takes place for 1.5, 1.7, 2.0 and 2.4 THz in Figure 5(a) and coincides exactly with the zero crossing of the rectified current in Figure 2(a). Finally, for higher frequencies the diphase is still increasing, so that most of the time in which the channel is open ($\Delta > 1$) the potential drop is negative and the current takes small (due to the low Δ) negative values, as observed in Figure 2(a). The described effect may be useful for frequency selectivity in detection and mixing applications.

3.3. Influence of the channel length

The standard strategy to optimize the frequency performance of the diodes is the reduction in their channel length, as reported in Figure 6. As L_C decreases, the rectifying response of the diodes extends to higher frequencies. In particular, the SSD with $L_C = 100$ nm is correctly responding up to frequencies over 2.0 THz, thus making possible the operation of these devices as, for example, power detectors of THz waves. After the first zero-crossing, the frequency for which the device does not work anymore depends on the channel length (in Figures 2 and 3 this frequency is always the same because L_C is constant). L_C is also found to largely influence the I–V curves. As observed in the inset of Figure 6, short-channel effects appear when the aspect ratio of the channel (L_C/W_C) decreases. In such a case, under reverse bias the potential of the lateral regions is not able to fully deplete the channel, so that the barrier preventing the current flow disappears and an inverse leakage current flows (as observed for $L_C = 100$ nm).

3.4. Link with the noise spectra

In previous works [11, 12] the MC analysis of the current noise spectral density in SSDs has evidenced the presence of a peak with a dependence on W_v analogous to that observed in the case of the rectifying response. To identify the similarities, in Figure 7 we compare the frequency

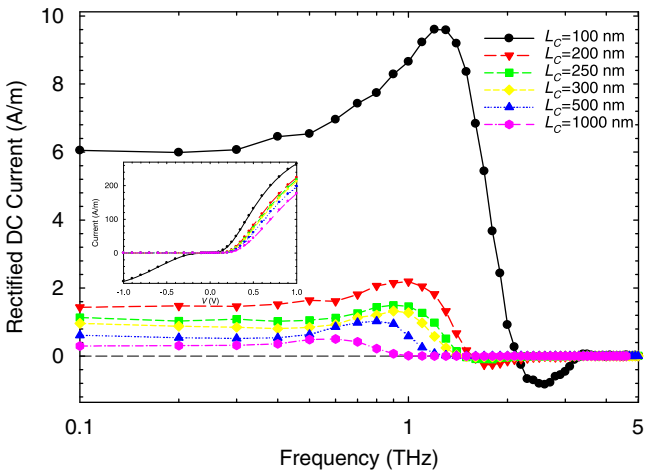

Figure 6. Mean current response vs frequency of the AC voltage ($V_0 = 0.25$ V) applied to the SSDs with $L_C = 100$, 200, 250, 300, 500 and 1000 nm. $W_C = 50$ nm, $W_h = W_v = 5$ nm, $\varepsilon_h = \varepsilon_v = 1$ and $L_{acc} = 175$ nm.

DOI: 10.1002/jnm

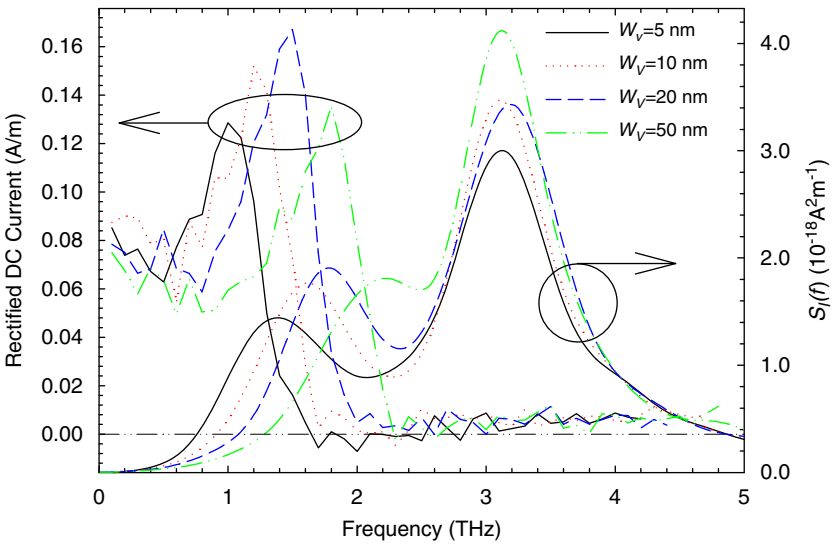

Figure 7. Comparison of the current noise spectra (right axis) calculated at equilibrium and the DC rectified current (left axis) when the amplitude of the AC excitation is 0.15 V for diodes with different W_v and $\varepsilon_v = 1$.

dependence of the current noise spectral density $S_I(f)$ (calculated at equilibrium) with that of the DC rectified current in SSDs with different W_v. Here the amplitude of the AC excitation is $V_0 = 0.15$ V, providing a sharper peak slightly shifted to higher frequencies (as compared with the results shown in Figure 2(a), where $V_0 = 0.25$ V). If we focus on the noise spectra, two peaks are observed. Plasma oscillations are the origin of the one appearing at the highest frequencies (above 3 THz, and independently of W_v) [11]. The other peak, at lower frequency (in the range 1–2 THz), exhibits a dependence on W_v quite similar to that observed in the DC rectified current. This indicates that, quite probably, we are observing the same microscopic phenomenon displayed in different macroscopic quantities.

The microscopic information provided by the MC simulations has allowed us to identify the origin of the low-frequency peak, which is the dynamics of the carriers reflected back at both sidewalls of the vertical trenches, so-called returning carriers [16]. In this phenomenon, electrons experience a deceleration/acceleration process at the potential barrier created by the surface charge at the interfaces of the vertical trenches, which originates charge density fluctuations at a characteristic frequency. As mentioned previously, the electron flow in the channel is mainly controlled by the charge present in this region of the device. On the other hand, the frequency dependence of $S_I(f)$ in log–log scale exhibits a distinct f^2 behavior [11], revealing a capacitive coupling of oscillations to the noise at the terminals. It means that a resonance in the collective charge fluctuations in the space-charge region around the vertical trenches becomes visible in the noise spectra (coupled to the terminals by the capacitance of the vertical trench C_v) and, what is more important from the point of view of applications, also in the DC response to AC excitations (due to the coupling to the channel via the horizontal trench). The resonance in the DC response takes place when the frequency of the excitation coincides with the characteristic frequency of the charge oscillations in the region near the vertical trench, whose dynamics is closely connected to plasma oscillations [13, 16]. In the study performed in Reference [13] the

DOI: 10.1002/jnm

origin of the resonance is attributed to localized surface plasma (LSP) oscillations, however, as explained in Reference [17] both are plausible interpretations because the plasma frequency appears explicitly in the characteristic time of a returning electron.

It must be borne in mind that the spectral density of current fluctuations at equilibrium is proportional to the small signal admittance of the device [18], while the DC response current is due to the rectifying behavior of the diode, corresponding to large signal operating conditions. On the other hand, the rectified current is shifted in frequency by the presence of the horizontal capacitor, while the noise is only sensitive to the vertical one (with no need of the presence of a conducting channel). All these facts explain why the frequency of the peak is not exactly the same in both quantities and why similarities are more pronounced for lower amplitude of the AC excitation (operation closer to small signal conditions). As concerns the 3D plasma peak around 3 THz observed in the noise spectra, it is originated by charge fluctuations in the access regions of the diode which, in contrast with the returning carrier fluctuations, do not couple to the conductance of the channel. That is the reason why it is present in the noise spectra and not in the DC rectified current.

The comparison of the rectified DC current in SSDs with different channel lengths (previously shown in Figure 6) with the corresponding noise spectra (not reported here) reveals again a parallel behavior of the frequency (f_p lower for longer channels) and relative amplitude of the low-frequency peak.

In order to confirm that the capacitance associated with the vertical trenches C_v is one of the key parameters of the resonance, two diodes with different values of W_v and ε_v, but adjusted to provide the same C_v, have been simulated (Figure 8). The current noise spectra are practically identical, thus supporting our interpretation.

As a conclusion of this section we have seen that in SSDs, by virtue of their particular geometry, a collective phenomenon leading to the appearance of noise (negative effect) couples to the DC to AC response and enhances the performance (positive effect).

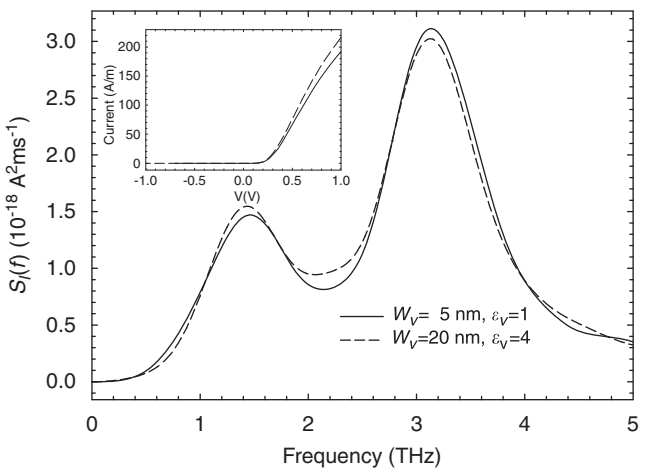

Figure 8. Current noise spectra calculated at equilibrium in diodes with different values of W_v and ε_v providing the same value of C_v. $W_v = 5$ nm, $\varepsilon_v = 1$ and $W_v = 20$ nm, $\varepsilon_v = 4$. The inset shows the corresponding I–V curves.

DOI: 10.1002/jnm

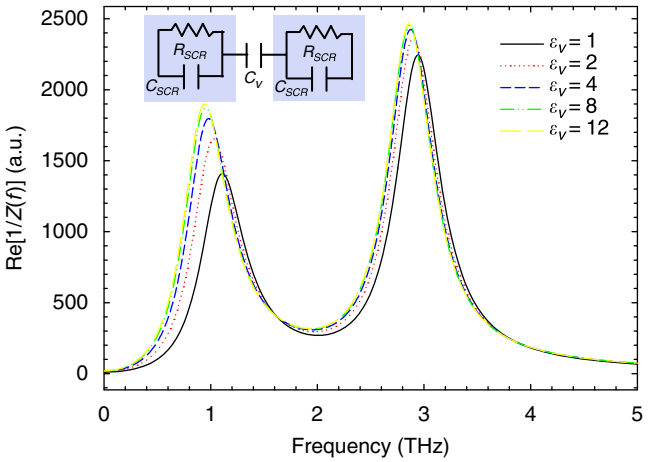

Figure 9. Real part of the admittance for diodes with different ε_v.

3.5. *Equivalent circuit*

Finally, by means of the equivalent circuit proposed in [11] we will explain the saturation in the shift of the low-frequency peak observed for $\varepsilon_v > 4$ in Figure 1(b). To this end, the noise spectra are determined in terms of the frequency dependence of the diode admittance $Y(f)$; $S_I(f) = 4K_BT\,\mathrm{Re}[Y(f)]$ at equilibrium. To model the space-charge region at both sides of the trenches, we include the presence of a capacitor and a resistance in parallel, R_{SCR} and C_{SCR}, respectively, placed in series with C_v, as drawn in the inset of Figure 9. C_{SCR} is the capacitance of the depletion region originated by the surface charges present at the vertical trenches. As a consequence of the series combination of C_v and C_{SCR}, the equivalent capacitance is fixed by the lowest one. Thus, when ε_v is increased above the limit in which C_v becomes much higher than C_{SCR} (what happens for $\varepsilon_v > 4$), the equivalent capacitance is practically C_{SCR}, so that the position of the low-frequency peak does not change, as observed in the spectra predicted by the equivalent circuit shown in Figure 9.

3.6. *Future trends*

We expect the amplitude and quality factor of the resonant peak observed in our calculations to be improved by enhancing the ballistic character of transport inside the diode. Additionally, it could be shifted to higher frequencies, quite interesting from the point of view of applications. Two approaches can be employed as future work: (i) simulate and fabricate SSDs with other small bandgap materials, such as InAs or InSb, with lower effective mass and higher mobility than InGaAs, and (ii) decrease the operation temperature. As an example, Figure 10 shows a preliminary simulation in which temperature is decreased from 300 to 77 K in InGaAs. A quite significant enhancement of the resonance is observed, improving the sensitivity of detection due to a superior mobility.

4. CONCLUSIONS

In this work we have shown that the resonant effects found in the noise and AC to DC rectification of SSDs are linked, being the same collective phenomenon that originates from the

DOI: 10.1002/jnm

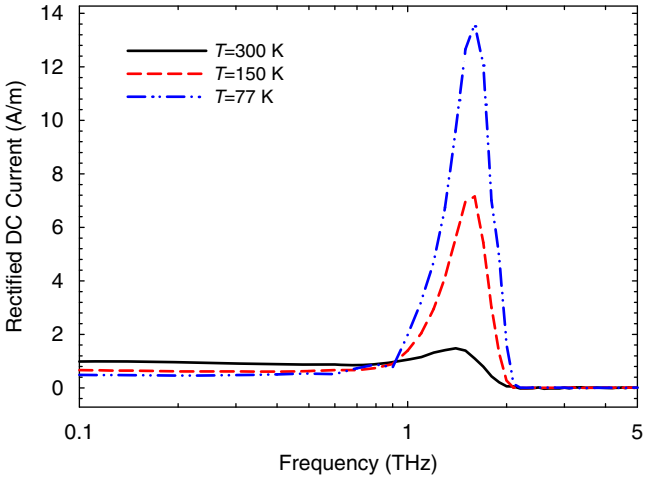

Figure 10. Mean current response vs frequency of the AC voltage ($V_0 = 0.25\,\mathrm{V}$) applied to an InGaAs-based SSD for different temperatures. $L_C = 250\,\mathrm{nm}$, $W_C = 60\,\mathrm{nm}$, $W_v = 20\,\mathrm{nm}$, $W_h = 5\,\mathrm{nm}$, $\varepsilon_h = \varepsilon_v = 1$ and $L_{acc} = 175\,\mathrm{nm}$.

presence of the peak in both quantities. Therefore, in this device the processes increase the current noise, with a characteristic frequency that can be controlled by the geometry, provide an enhancement of its response to AC signals. This fact allows thinking of applications of SSDs as detectors of THz signals with a certain degree of frequency selectivity tuned by geometry of the diodes (width or dielectric material of the vertical trenches). They can also be quite useful for broadband operation because devices with different geometries can be fabricated on the same chip.

ACKNOWLEDGEMENTS

This work has been partially supported by the Dirección General de Investigación (MEC, Spain), by FEDER through the Project No. TEC2007-61259/MIC, and by the Consejería de Educación of the Junta de Castilla y León (Spain) through the Project No. SA019A08.

REFERENCES

1. *Terahertz Frequency Detection and Identification of Materials and Objects*, Miles RE, Zhang X-C, Eisele H, Krotkus A (eds). Springer: New York, 2007.
2. Knap W, Teppe F, Dyakonova N, Coquillat D, Łusakowski J. Plasma wave oscillations in nanometer field effect transistors for terahertz detection and emission. *Journal of Physics*: *Condensed Matter* 2008; **20**:384205.
3. El Fatimy A, Teppe F, Dyakonova N, Knap W, Seliuta D, Valusis G, Shchepetov A, Roelens Y, Bollaert S, Cappy A, Rumyantsev S. Resonant and voltage-tunable terahertz detection in InGaAs/InP nanometer transistors. *Applied Physics Letters* 2006; **89**:131926.
4. Łusakowski J, Knap W, Dyakonova N, Varani L, Mateos J, González T, Roelens Y, Bollaert S, Cappy A, Karpierz K. Voltage tuneable terahertz emission from a ballistic nanometer InGaAs/InAlAs transistor. *Journal of Applied Physics* 2005; **97**:064307.
5. Gruzinskis V, Shiktorov P, Starikov E, Reggiani L, Varani L, Vaissiere JC. Free-carrier grating and terahertz generation from InN n^+nn^+ structures under treaming plasma instability. *Semiconductor Science and Technology* 2004; **19**:S173.

DOI: 10.1002/jnm

6. Starikov E, Shiktorov P, Gruzinskis V, Varani L, Palermo C, Millithaler JF, Reggiani L. Terahertz generation in nitrides due to transit-time resonance assisted by optical phonon emission. *Journal of Physics*: *Condensed Matter* 2008; **20**:384209.
7. Song AM, Missous M, Omling P, Peaker AR, Samuelson L, Seifert W. Unidirectional electron flow in a nanometer-scale semiconductor channel: A self-switching device. *Applied Physics Letters* 2003; **83**:1881.
8. Mateos J, Vasallo BG, Pardo D, González T. Operation and high-frecuency performance of nanoscale unipolar rectifying diodes. *Applied Physics Letters* 2005; **86**:212103.
9. Balocco C, Song AM, Åberg M, Forchel A, González T, Mateos J, Maximov I, Missous M, Rezazadeh AA, Saijets J, Samuelson L, Wallin D, Williams K, Worshech L, Xu HQ. Microwave detection at 110 GHz by nanowires with broken symmetry. *Nano Letters* 2005; **5**:1423.
10. Balocco C, Halsall H, Vinh NQ, Song AM. THz operation of asymmetric-nanochannel devices. *Journal of Physics*: *Condensed Matter* 2008; **20**:384203.
11. Iñiguez-de-la-Torre I, Mateos J, Pardo D, González T. Monte Carlo study of noise spectra in self-switching nanodiodes. *Journal of Applied Physics* 2008; **103**:024502.
12. Xu KY, Lu XF, Song AM, Wang G. Terahertz harmonic generation using a planar nanoscale unipolar diode at zero bias. *Applied Physics Letters* 2008; **92**:163503.
13. Xu KY, Lu XF, Song AM, Wang G. Enhanced terahertz detection by localized surface plasma oscillations in a nanoscale unipolar diode. *Journal of Applied Physics* 2008; **103**:113708.
14. Mateos J, Vasallo BG, Pardo D, González T, Galloo JS, Roelens Y, Bollaert S, Cappy A. Ballistic nanodevices for terahertz data processing: Monte Carlo simulations. *Nanotechnology* 2003; **14**:117.
15. Varani L, Reggiani L, Kuhn T, González T, Pardo D. Microscopic simulation of electronic noise in semiconductor materials and devices. *IEEE Transactions on Electron Devices* 1994; **41**:1916.
16. Trippe M, Bosman G, Van der Ziel A. Transit-time effects in the noise of Schottky–barrier diodes. *IEEE Transactrions on Microwave Theory Techniques* 1986; **34**:1183.
17. Iñiguez-de-la-Torre I, Mateos J, Pardo D, Song AM, González T. Noise and THz rectification linked by geometry in planar asymmetric nanodiodes. *Applied Physics Letters* 2009; **94**:093512.
18. González T, Mateos J, Pardo D, Varani L, Reggiani L. Injection statistics simulator for dynamic analysis of noise in mesoscopic devices. *Semiconductor Science and Technology* 1999; **14**:L37.

AUTHORS' BIOGRAPHIES

Ignacio Iñiguez-de-la-Torre was born in Valladolid, Spain, in 1981. He received the BS and PhD degrees in Physics from the University of Salamanca in 2004 and 2008, respectively. Since 2004, he has been working with the Electronics Group, Department of Applied Physics, University of Salamanca, as a Grant Holder. He worked for three months at the Institut d'Electronique, de Microélectronique et de Nanotechnologies (IEMN), France in 2007 and another three moths in the School of Electrical and Electronic Engineering in the University of Manchester, United Kingdom in 2008. In September 2009, he became a Postdoctoral Research Associate in the Department of Electrical and Computer Engineering at the University of Massachusetts in Lowell. His research interest is in the development of novel device concepts using ballistic transport for THz data processing.

Javier Mateos was born in Salamanca, Spain, in 1970. He received the BS and PhD degrees in Physics from the University of Salamanca in 1993 and 1997, respectively. Since 1993 he has been working in the Department of Applied Physics of the University of Salamanca, becoming Associate Professor in 2000. His present research interests are in the development of novel device concepts using ballistic transport, THz devices and HEMTs based on both narrow and wide bandgap III–V semiconductors. He is the author or co-author of more than 80 refereed scientific journal papers and 130 conference presentations.

DOI: 10.1002/jnm

Daniel Pardo was born in Valladolid, Spain, in 1946. He graduated in Physics in 1971 from the University of Valladolid, where he also received the PhD degree in 1975. From 1971 to 1981 he was working in the Electronics Department of the University of Valladolid on the characterization of semiconductor materials and modeling of semiconductor devices, where he was promoted as Associate Professor in 1978. In 1981 he joined the Applied Physics Department of the University of Salamanca, where he is Full Professor since 1983, and the Head of the Semiconductor Devices Research group. His current research interest is the Monte Carlo simulation of III–V semiconductor devices.

Aimin Song received his PhD degree from the Chinese Academy of Sciences in 1995. After three years of fellowships at University of Glasgow and University of Munich awarded by the Royal Society and the Alexander von Humboldt foundation, he worked at Lund University as a Swedish Natural Science Research Council Open Postdoc and then as a Guest Lecturer. He moved to Manchester as a Lecturer in 2002, and became Professor of Nanoelectronics in 2006. His research is to explore novel nanodevice concepts, particularly ultra-high-speed nano-diodes and transistors, for printed electronics as well as energy harvesting. Recently, he received a Royal Society Brian Mercer Feasibility Award and Distinguished Achievement Medal for 'Researcher of the Year 2007' of the University of Manchester. He is the Founding Director of a spin-out company, Nano ePrint Ltd.

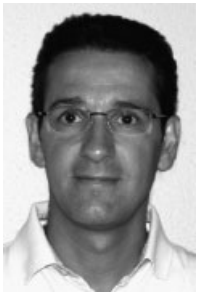

Tomás González was born in Salamanca, Spain, in 1967. He graduated in Physics from the University of Salamanca in 1990, where he received the PhD degree in Physics in 1994. Since 1991 he has been working in the Department of Applied Physics at the University of Salamanca, where he is currently Full Professor of Electronics. His main research activity is in the field of electronic transport in semiconductor materials and high-frequency electronic devices, with special application to the modeling of electronic noise by microscopic approaches. Recently he has also been involved in the development of novel device concepts based on ballistic transport to operate in the THz range. He is the author or co-author of more than 120 refereed scientific journal papers and 160 conference presentations.

DOI: 10.1002/jnm